

An Allele-Centric Pan-Graph-Matrix Representation for Scalable Pangenome Analysis

Roberto Garrone
University of Milano-Bicocca, Italy
`roberto.garrone@unimib.it`

Abstract

Population-scale pangenome analysis increasingly requires representations that unify single-nucleotide and structural variation while remaining scalable across large cohorts. Existing formats are typically sequence-centric, path-centric, or sample-centric, and often obscure population structure or fail to exploit carrier sparsity. We introduce the H1 pan-graph-matrix, an allele-centric representation that encodes exact haplotype membership using adaptive per-allele compression. By treating alleles as first-class objects and selecting optimal encodings based on carrier distribution, H1 achieves near-optimal storage across both common and rare variants. We further introduce H2, a path-centric dual representation derived from the same underlying allele–haplotype incidence information that restores explicit haplotype ordering while remaining exactly equivalent in information content. Using real human genome data, we show that this representation yields substantial compression gains, particularly for structural variants, while remaining equivalent in information content to pangenome graphs. H1 provides a unified, population-aware foundation for scalable pangenome analysis and downstream applications such as rare-variant interpretation and drug discovery.

Keywords: Pangenome representation; Allele-centric modeling; Genomic variation graphs; Sparse–dense hybrid encoding; Structural variants; Population-scale genomics; Genomic data compression

1 An Allele-Centric Pan-Graph-Matrix Representation

The H1 pan-graph-matrix is not simply another instance of a binary matrix applied to genomic data. Its novelty lies in a redefinition of the unit of representation and in the adaptive manner in which population-scale genomic relationships are encoded. The contribution of H1 emerges at the intersection of pangenome modeling, compression-aware data representation, and population-level genomic analysis, where existing representations exhibit structural limitations [12, 6]. While recent work has substantially expanded catalogs of structural variation and enabled graph-based human pangenome references [2, 11], scalable representations that make population-level allele incidence explicit remain an open challenge.

Binary incidence matrices are a well-established mathematical construct and have appeared in multiple areas of genomics. However, H1 departs from prior approaches by redefining what constitutes a row of the matrix and how that row is stored. In H1, each row corresponds to a concrete genomic allele, whether arising from a single-nucleotide variant or a structural variant, rather than to a genomic site, a sample, or a haplotype path. Each row encodes exact haplotype membership for that allele and is stored using an encoding strategy chosen independently for that row. This per-allele adaptivity is central to the design: alleles are treated as first-class population objects whose representation is driven by their carrier structure rather than by a fixed global format.

Most existing genomic data representations implicitly fix both the semantic unit and the encoding scheme. Variant-centric formats such as VCF or BCF organize data by genomic position and record genotypes per sample using a rigid layout [4]. While effective for sample-centric queries, these formats are poorly aligned with population-level questions that require enumerating carriers of specific alleles. In contrast, H1 stores alleles as rows and provides direct access to the set of haplotypes carrying a given allele. As a consequence, compression efficiency in H1 follows population incidence patterns rather than file format constraints. Dense representations can also be implemented using compressed bitmap schemes [3], which reduce constant factors but do not alter the underlying dense–sparse trade-off that governs the choice of representation.

H1 also differs fundamentally from haplotype-centric compression methods such as those based on the positional Burrows–Wheeler transform. These approaches are optimized for compressing entire haplotypes and excel in tasks such as phasing and imputation [5, 9], but they make allele-centric queries difficult to express efficiently. This limitation is particularly relevant for structural variants, whose population-scale diversity and functional impact have been highlighted by large multi-platform studies [2]. H1 deliberately avoids compressing haplotypes and instead compresses the incidence relation between alleles and haplotypes, shifting the representation from a path-centric to a relation-centric view. This distinction explains why H1 remains effective across both single-nucleotide and structural variants and complements existing haplotype compressors.

Graph-based pangenome representations encode genomic alternatives through nodes, edges, and paths, making structural rearrangements explicit and supporting alignment and traversal operations [7, 10]. However, population structure is implicit in these graphs, and compression is primarily driven by sequence redundancy rather than by carrier sparsity. The pan-graph-matrix can be understood as the incidence algebra of the pangenome graph: each alternative path corresponds to one or more rows of the matrix, and each haplotype path corresponds to a column. Both representations are equivalent in information content with respect to allele–haplotype incidence and ordered haplotype traversals, but emphasize different analytical dimensions.

A key property of H1 is its adaptive encoding strategy. For each allele, the representation selects between a dense bitmap and a sparse carrier list based on a break-even threshold that can be derived from a simple encoding cost model and depends on cohort size. Empirically, this threshold follows the relation

$$k^* \approx \frac{H}{\log_2 H},$$

where H denotes the number of haplotypes and k^* the carrier count at which dense and sparse encodings are equally efficient. This relation reflects a structural property of the encoding problem arising from population-scale allele incidence patterns, rather than an implementation artifact. By exploiting this trade-off directly, H1 achieves compression that closely tracks the lower envelope of dense and sparse encodings across the allele frequency spectrum, including regimes dominated by rare and structural variants.

In summary, H1 introduces an allele-centric, population-aware representation of pangenomic variation that departs fundamentally from sequence-centric, path-centric, and sample-centric approaches. By combining this perspective with an adaptive, cost-model-grounded encoding strategy, H1 unifies graph and matrix views of the pangenome and provides a scalable foundation for representing both single-nucleotide and structural variation in population-scale datasets.

1.1 Encoding cost model and break-even threshold

The adaptive encoding strategy used in H1 is based on a simple cost comparison between dense and sparse representations of allele–haplotype incidence. Let H denote the number of haplotypes

Representation	Primary unit	Carrier queries	Ordering/topology	Compression driver
VCF / BCF	Genomic site	Indirect	Implicit	File-level encoding
PBWT-based	Haplotype	Limited	Explicit	Haplotype similarity
Pangenome graphs	Graph node/edge	Implicit	Explicit	Sequence redundancy
H1 (this work)	Allele	Direct	No	Carrier sparsity
H2 (this work)	Haplotype path	Indirect	Direct	Path abstraction

Table 1: Comparison of common genomic representations. H1 and H2 form a dual pair: H1 makes allele–haplotype incidence explicit and compressible by sparsity, while H2 restores ordered haplotype paths without duplicating population-level incidence information.

in the cohort and let k denote the number of haplotypes carrying a given allele.

In a dense bitmap representation, the incidence of an allele is encoded as a bit vector of length H , yielding a storage cost

$$C_{\text{dense}}(H) = H \text{ bits},$$

up to constant overheads for alignment or headers.

In a sparse representation, the same information is encoded as an explicit list of the k haplotype identifiers carrying the allele. Assuming fixed-width integer identifiers, the storage cost is

$$C_{\text{sparse}}(k, H) = k \lceil \log_2 H \rceil \text{ bits.}$$

Variable-length integer encodings or compressed list representations change constant factors but preserve the same asymptotic dependence on k and H .

Equating the two costs yields a break-even carrier count

$$k^* \approx \frac{H}{\log_2 H},$$

at which dense and sparse encodings incur comparable storage costs. Alleles with $k \ll k^*$ are therefore more efficiently represented as sparse lists, while alleles with $k \gg k^*$ favor dense bitmaps.

This threshold is not specific to a particular dataset but follows from the structure of the encoding family considered. Correlations between haplotypes, population stratification, or alternative integer coding schemes affect compression constants but do not alter the qualitative crossover between sparse and dense regimes. In practice, H1 selects the encoding that minimizes storage cost for each allele independently, yielding compression behavior that closely tracks this lower envelope across the allele frequency spectrum.

2 Matrix–Graph Correspondence

The schematic in Figure 1 illustrates the correspondence between a pangenome graph representation and the pan-graph-matrix formalism. On the left, a reference backbone is augmented with alternative paths representing genomic variation. Each bubble in the graph encodes mutually exclusive alleles at a locus, and haplotypes are represented implicitly as paths traversing the graph. Structural variants give rise to long alternative branches, while single-nucleotide variants correspond to short deviations from the reference path.

On the right, the same information is expressed in matrix form. Each row corresponds to a concrete allele represented in the graph, and each column corresponds to a haplotype. A non-zero entry indicates that the haplotype path traverses the branch associated with that allele in the

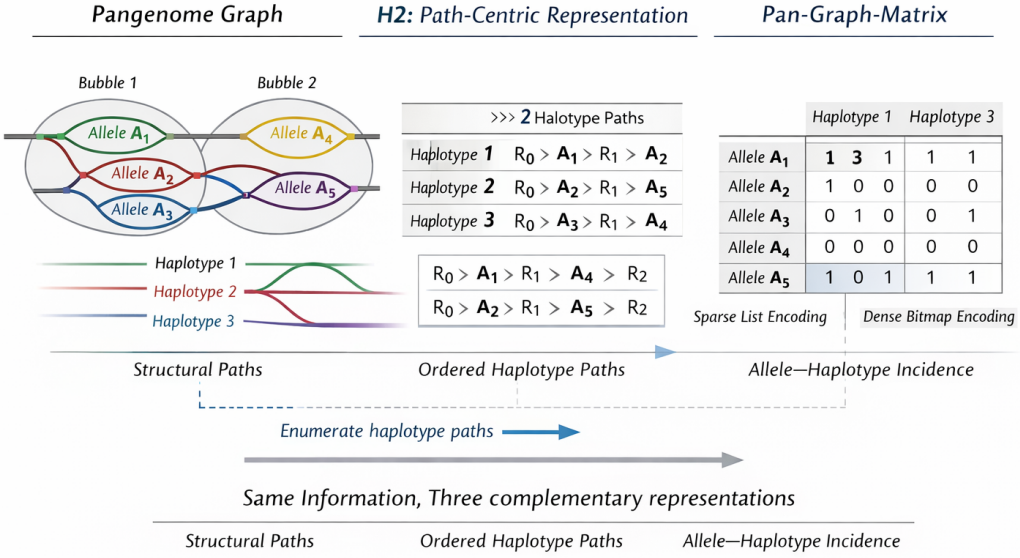


Figure 1: Schematic correspondence between three information-equivalent pangenome representations. (*Left*) A pangenome graph encodes structural alternatives as bubbles and haplotypes as implicit paths. (*Center*) The H2 path-centric representation makes haplotype paths explicit as ordered sequences of reference and alternative segments. (*Right*) The pan-graph-matrix (H1) encodes allele–haplotype incidence, with rows corresponding to alleles and columns to haplotypes, stored using adaptive sparse or dense encodings based on carrier distribution. Together, the graph, H2, and H1 representations encode the same underlying genomic variation while emphasizing complementary dimensions: structural topology, haplotype ordering, and population incidence.

graph. In this view, graph topology is abstracted away, and population structure becomes explicit through the sparsity pattern of the matrix.

The figure highlights how alleles with few carriers give rise to sparse rows, while common alleles produce dense rows. This observation motivates the adaptive encoding strategy used in H1, where each row is stored either as a sparse carrier list or as a dense bitmap depending on its carrier count. Importantly, no information is lost in moving between the graph and matrix views: haplotype paths in the graph are in one-to-one correspondence with columns of the matrix, and alternative graph branches correspond to matrix rows. Equivalence here is with respect to the allele–haplotype incidence relation and ordered haplotype traversals over the same set of allelic alternatives; sequence payloads are orthogonal to this representation and can be attached as annotations when required.

This duality emphasizes the complementary roles of the two representations. The graph view makes structural alternatives and genomic context explicit, supporting visualization and traversal, while the pan-graph-matrix exposes population incidence directly, enabling efficient compression and population-level queries. Together, they provide two perspectives on the same underlying pangenomic information, optimized for different analytical tasks.

All experiments were conducted on phased SNV/INDEL and structural variant callsets from the 1000 Genomes Project 30 \times high-coverage sequencing data [1]. Quantitative compression results for

Table 2: Compression by variant class for a 2 Mb region on chromosome 1 using 200 diploid individuals (400 haplotypes). List-only encodings are omitted for clarity.

Variant class	Sites	Bitmap (bits)	Hybrid (bits)	Hybrid / Bitmap
SNV / INDEL	24,921	9.97M	3.11M	0.31
Structural variants	45	18k	3.98k	0.22

the same genomic region are reported in Table 2. For a 2 Mb window on chromosome 1 comprising 200 diploid individuals (400 haplotypes), single-nucleotide and short insertion–deletion variants account for 24,921 sites, while only 45 sites correspond to true structural variants after filtering by SVTYPE. Despite their small number, structural variants exhibit an extreme sparsity regime: more than half are carried by two or fewer haplotypes, and nearly 87% have allele frequency below 10%.

In this regime, the adaptive hybrid encoding used by H1 achieves a 78% reduction in storage relative to a bitmap-only representation for structural variants, substantially exceeding the compression gains observed for SNVs in the same cohort. This behavior follows directly from the carrier sparsity of structural variants and aligns with the theoretically predicted break-even threshold between dense and sparse encodings. By contrast, SNVs occupy a mixed regime in which both sparse and dense representations are frequently selected, resulting in a more moderate but still substantial reduction in storage.

When SNV and structural-variant H1 representations are merged, the resulting structure contains 24,966 sites, corresponding exactly to the sum of 24,921 SNVs and 45 true structural variants. As expected, the overall compression statistics of the merged representation closely match those of the SNV-only case, since the contribution of 45 structural variants is negligible relative to approximately 25,000 SNVs. This confirms that the merging procedure preserves correctness and that compression behavior is dominated by the most numerous variant class.

From a graph-construction perspective, this observation has important implications. A naive pangenome graph that materializes a backbone break for every SNV produces an extremely fine-grained structure with tens of thousands of segments and bubbles, which is difficult to visualize and interpret. In practice, pangenome tools avoid this representation by encoding SNVs implicitly or by compressing chains of variants along the reference path.

For visualization and topological analysis, a structural-variant–focused graph is therefore preferable. In this construction, the reference backbone is segmented only at structural-variant breakpoints, while SNVs are treated as annotations rather than explicit graph nodes. This yields a compact graph with a small number of reference segments and clearly identifiable bubbles corresponding to large genomic rearrangements. An intermediate alternative is a coarsened SNV graph, in which the backbone is segmented at fixed genomic intervals (for example every 1 kb) in addition to structural-variant boundaries, and SNVs are attached as side nodes without splitting the reference path at single-base resolution. This approach preserves variant localization while keeping graph size manageable.

Together, the compression results and graph constructions illustrate how the pan-graph-matrix and the pangenome graph provide complementary views of the same data. The matrix representation explains scalability and compression behavior through population-level sparsity, while the graph representation supports structural interpretation and visualization when appropriate levels of abstraction are chosen.

In algebraic terms, the pan-graph-matrix can be interpreted as the incidence algebra of the

pangenome graph. While the graph representation makes explicit where alternative genomic realizations exist and how they connect through nodes and edges, the pan-graph-matrix encodes the incidence relation between alleles and haplotypes, making explicit which haplotypes realize each alternative. Each bubble or alternative path in the graph corresponds to one or more rows of the matrix, and each traversal of that bubble by a haplotype corresponds to a non-zero entry. This correspondence is exact rather than approximate: the graph encodes structural and ordering relationships, whereas the matrix encodes population realization. Framed in this way, the two representations are information-equivalent but emphasize complementary analytical dimensions.

2.1 H2: A Path-Centric Dual Representation

While the H1 pan-graph-matrix provides an allele-centric, population-aware view optimized for scalable analysis and compression, certain classes of questions require explicit ordering information along haplotypes. To address this need without abandoning the allele-centric abstraction, we introduce $H2$, a path-centric dual representation derived directly from H1.

In H2, each haplotype is represented as an ordered sequence of abstract graph edges corresponding to reference segments and variant-induced alternatives. Conceptually, H2 restores the notion of haplotype paths that is implicit in pangenome graphs, while maintaining a strict correspondence with the allele–haplotype incidence encoded in H1. An inverted index maps each edge to the set of haplotypes that traverse it, enabling efficient queries over adjacency, ordering, and local topology.

Crucially, H1 and H2 are information-equivalent. For any allele represented as a row in H1, the set of haplotypes carrying that allele is exactly equal to the set of haplotypes whose paths traverse the corresponding edges in H2. Conversely, ordered haplotype paths in H2 can be reconstructed from the same underlying data used to build H1. The two representations therefore encode the same pangenome, but project it along complementary analytical dimensions.

This duality establishes a principled separation of concerns. H1 emphasizes population structure, carrier sparsity, and scalable compression, making it well suited for population-level statistics, rarity analysis, and cohort queries. H2 emphasizes haplotype ordering and topology, supporting analyses that depend on local genomic context, such as neighborhood inspection around structural variants or reconstruction of variant sequences along individual haplotypes. By keeping these concerns separate yet linked through exact equivalence, the framework avoids conflating population incidence with path structure while preserving access to both.

In this sense, the pan-graph-matrix can be interpreted as the incidence algebra of the pangenome graph: the graph encodes where alternative genomic realizations exist and how they connect, whereas H1 encodes which haplotypes realize each alternative, and H2 restores the ordered realization of these alternatives along haplotypes. Together, H1 and H2 provide complementary, information-preserving views of the same underlying pangenomic variation, each optimized for a distinct class of analytical tasks.

2.2 Operations enabled by H1 and H2

Beyond storage, the H1 and H2 representations support a small set of primitive operations that are central to population-scale pangenome analysis. The cost of these operations depends primarily on the carrier count k of an allele and the total number of haplotypes H . Query-oriented genotype stores [8] optimize specific access patterns over large cohorts but retain sample- or haplotype-centric layouts, whereas H1 and H2 expose allele incidence and path structure directly. Further, these operations illustrate how H1 emphasizes population incidence and set-based queries, while H2 restores ordering and topological context. Together, they support a range of analytical tasks

without conflating population-level incidence with path structure.

Carrier enumeration. Given an allele represented as a row of H1, enumerating all haplotypes carrying that allele requires $O(k)$ time for sparse rows and $O(H/w)$ time for dense rows, where w is the machine word size. In practice, dense rows can exploit bit-iteration primitives to enumerate set bits efficiently.

Allele frequency computation. Allele frequency is obtained directly as k/H for sparse rows or via a population count operation on dense bitmaps. This avoids scanning per-sample genotype records.

Carrier set intersection. Intersecting the carriers of two alleles can be performed by merging two sparse lists in $O(k_1 + k_2)$ time, by bitwise conjunction of two dense bitmaps in $O(H/w)$ time, or by iterating the smaller representation and testing membership in the larger. This supports cohort stratification and multi-allele filtering.

Cohort filtering and stratification. More complex filters involving multiple alleles can be implemented as successive intersections with early termination. The adaptive encoding of H1 ensures that operations involving rare alleles typically operate in the sparse regime.

Haplotype path reconstruction and local context queries. Using H2, ordered haplotype paths can be reconstructed by traversing the sequence of reference and alternative segments associated with a given haplotype. Local neighborhood queries around a structural variant can therefore retrieve both carrier sets (via H1) and ordered genomic context (via H2) without materializing full pangenome graphs.

Potential applications

The representations introduced in this work are designed as general-purpose infrastructure for population-scale pangenome analysis, and their potential applications extend across several domains. In particular, allele-centric incidence enables efficient identification and stratification of rare and structural variants, which are of interest in pharmacogenomics and precision medicine workflows. More broadly, the explicit separation between population incidence (H1) and haplotype ordering (H2) supports cohort-level analyses, population stratification, and exploratory studies that combine variant presence with local genomic context. Because the core representations encode relational structure independently of nucleotide sequence payloads, they are also compatible with privacy-aware data sharing scenarios in which sequence data are restricted or attached as external annotations. Concrete application-specific pipelines and benchmarks are left to future work.

Data Availability

All analyses were performed using publicly available variant callsets from the 1000 Genomes Project high-coverage ($30\times$) sequencing data aligned to GRCh38, generated by the New York Genome Center and released via the International Genome Sample Resource. Phased SNV/INDEL and structural variant VCFs were obtained from the 2020 high-coverage release. No controlled-access data were used.

3 Graph-based visualizations of the H1 pangenome

To illustrate the structural properties of the inferred pangenome and to clarify how different levels of abstraction arise from the same underlying representation, we generated two complementary GFA-like visualizations of a 2 Mb region on chromosome 1. Both graphs are derived from the same H1 pan-graph-matrix encoding and differ only in how the reference backbone is segmented, thereby emphasizing distinct aspects of genomic variation without altering the underlying information content. The difference in abstraction level between the two graph constructions is reflected directly in their size. In the SV-backbone graph, segmenting the reference only at structural-variant breakpoints yields 91 reference segments connected by 90 edges, with each bubble corresponding to a true structural variant. In contrast, the coarse pangenome graph produced by 1 kb tiling in addition to structural-variant boundaries contains 2,090 reference segments, resulting in a substantially larger and denser topology. These counts illustrate how graph size scales with backbone segmentation granularity rather than with the underlying allele–haplotype incidence, which remains unchanged. The choice of a 1 kb tiling resolution represents a pragmatic trade-off between positional resolution and graph complexity, preserving approximate variant localization while keeping graph size manageable for visualization and inspection. Alternative tiling resolutions provide a continuous trade-off between resolution and graph size and are left to future work.

The first visualization is an SV-backbone graph with SNV annotations (Figure 2). In this construction, the reference backbone is segmented exclusively at structural-variant breakpoints, yielding 91 reference segments across the region. The 45 true structural variants identified in this window are represented as alternative paths (bubbles) connecting backbone segments. Single-nucleotide variants are not used to split the backbone; instead, they are retained as annotations associated with the corresponding reference segments.

As a result, the graph remains compact, largely linear, and easy to interpret. Each bubble corresponds to a true structural variant, and the overall topology directly reflects large-scale genomic rearrangements such as insertions and deletions. This representation is particularly well suited for topological inspection and explanatory visualization, as it highlights how structural variants reshape the reference path without overwhelming the visualization with fine-scale variation. The small number of nodes and edges visible in the graph directly reflects the rarity and sparsity of structural variants in the cohort.

The second visualization is a coarse pangenome graph incorporating both single-nucleotide variants and structural variants (Figure 3). Here, the reference backbone is segmented using a coarse tiling strategy with 1 kb intervals, in addition to structural-variant boundaries, producing 2,090 reference segments across the same region. Structural variants are again represented as bubbles between segments, while single-nucleotide variants are attached as short alternative nodes connected to their corresponding backbone segments rather than splitting the reference path at single-base resolution.

This graph contains the full set of approximately 25,000 single-nucleotide variants together with the 45 structural variants, making it substantially denser and visually more complex. The resulting crowded appearance is a faithful reflection of the underlying variation rather than a limitation of the model. However, direct visualization of the complete graph is less informative without filtering or sampling. Meaningful inspection therefore requires selective display, for example by focusing on structural variants or on a random subset of single-nucleotide variants.

Taken together, these two visualizations demonstrate how different graph constructions serve complementary analytical purposes. The SV-backbone graph provides a clean and interpretable view of large-scale genomic structure, while the coarse pangenome graph captures the full spectrum of variation at the cost of visual complexity. Importantly, both graphs are derived from the same H1

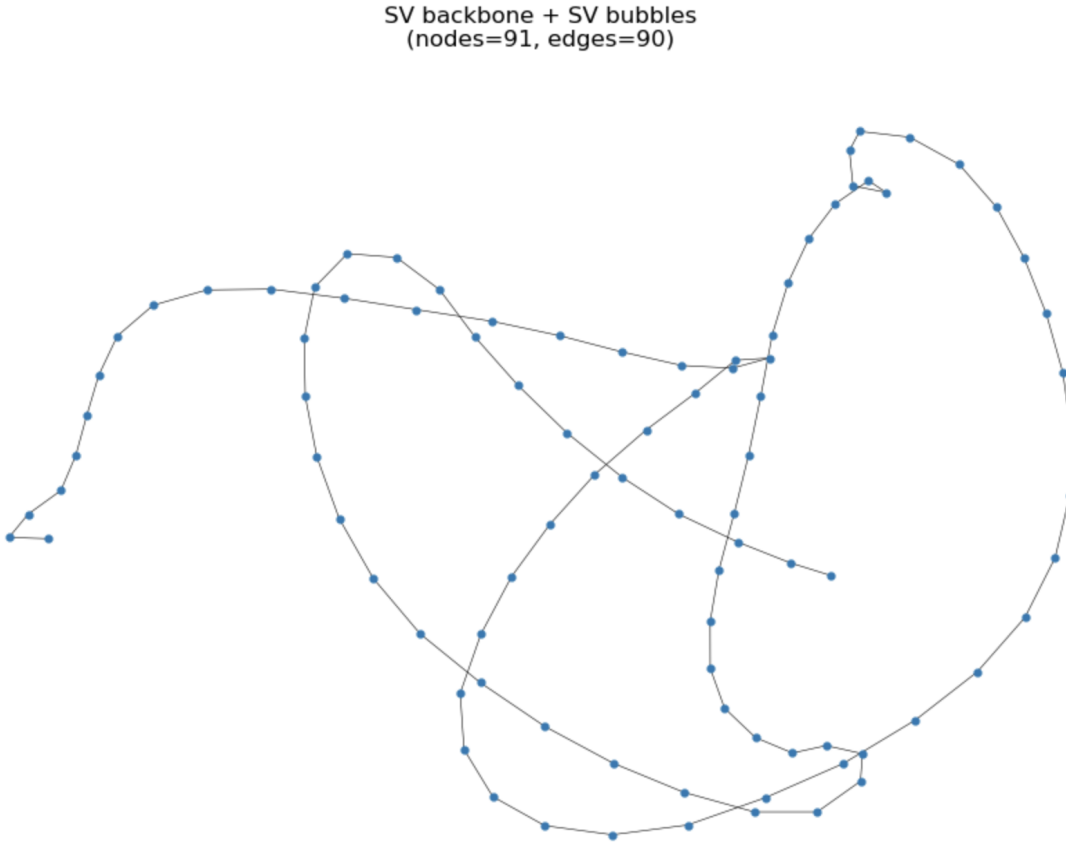


Figure 2: SV-backbone pangenome graph for a 2 Mb region on chromosome 1 derived from the H1 pan-graph-matrix. The reference backbone is segmented exclusively at structural-variant breakpoints, resulting in 91 reference segments across the region. Forty-five true structural variants are represented as alternative paths (bubbles) connecting backbone segments. Single-nucleotide variants are not used to split the backbone and are instead retained as annotations associated with the corresponding reference segments. This representation yields a compact, largely linear graph in which each bubble corresponds to a true structural rearrangement, making the large-scale genomic structure easy to interpret.

encoding and differ only in backbone segmentation, illustrating the flexibility of an allele-centric, relation-based pangenome representation in supporting multiple levels of abstraction. This flexibility mirrors the compression behavior observed in the pan-graph-matrix, where sparse structural variants and dense single-nucleotide variants coexist within a unified representation while being treated optimally according to their population incidence.

4 Structure-Aware Compression of Graph Paths

Haplotype paths in pangenome graphs are not arbitrary symbol sequences: they are constrained walks over a directed graph with strong local dependencies. Exploiting these dependencies is essential to approach the information-theoretic lower bound on compressibility. The implemented compressor explicitly models each path as a realization of a first-order Markov process over graph nodes, capturing local transition regularities without requiring global enumeration of all possible

Coarse graph: ref + SV + sampled SNVs
(nodes=2435, edges=2479)

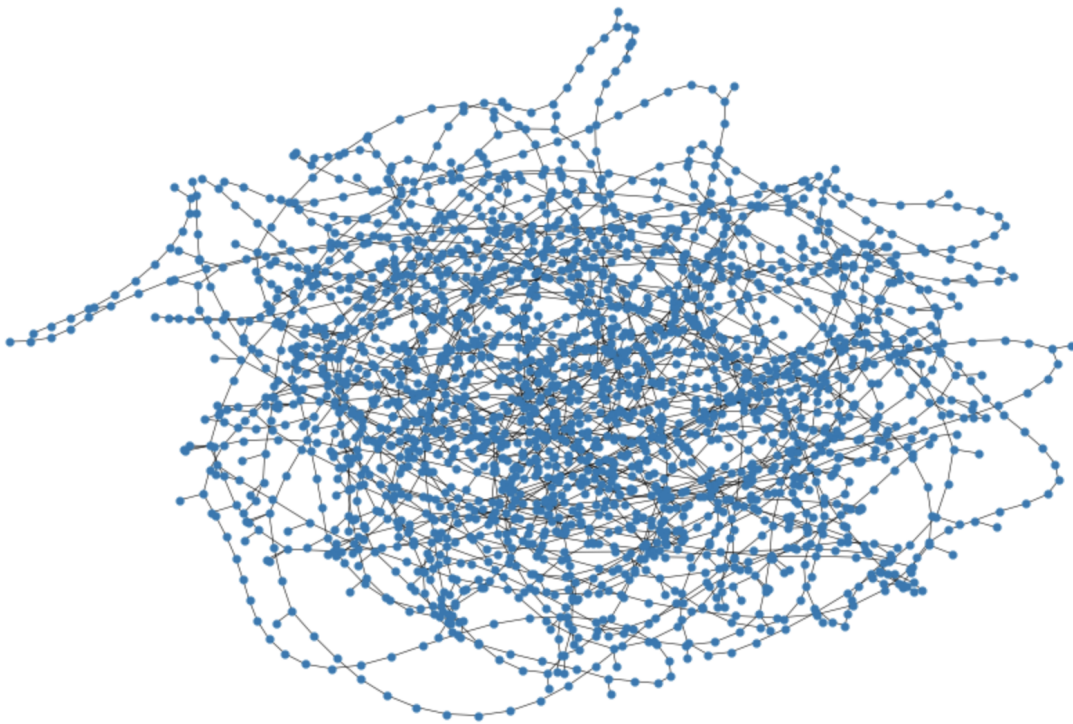


Figure 3: Coarse pangenome graph for the same 2 Mb region on chromosome 1 incorporating both single-nucleotide variants and structural variants. The reference backbone is segmented using 1 kb intervals in addition to structural-variant boundaries, producing 2,090 reference segments. Structural variants are represented as alternative paths between segments, while approximately 25,000 single-nucleotide variants are attached as short alternative nodes without splitting the backbone at single-base resolution. The resulting graph is substantially denser and visually crowded, faithfully reflecting the full spectrum of genomic variation in the region. Meaningful inspection therefore requires selective filtering or sampling, for example by focusing on structural variants or a subset of single-nucleotide variants.

paths.

4.1 Entropy-Optimal Coding with Minimal Overhead

By employing context-dependent Huffman coding, the compressor achieves expected code lengths within one bit of the Shannon entropy for each contextual distribution. Unlike naïve per-edge encodings, this approach avoids systematic over-penalization of high-probability transitions, which are prevalent in real haplotype data. At the same time, Huffman coding avoids the numerical instability and implementation complexity associated with arithmetic coding or ANS, while still providing strong entropy guarantees. This makes the method particularly well suited to sparse, skewed distributions typical of pangenome transitions.

4.2 Sparsity Preservation and Scalability

A key design choice is to restrict each context alphabet to its empirically observed support. This has two important consequences:

- the cost of building and storing codebooks scales with observed transitions rather than with the total number of graph nodes;
- memory usage remains linear in the number of distinct transitions present in the dataset.

This sparsity-aware construction is critical for large H2 instances, where full-alphabet models would be prohibitively expensive and largely uninformative.

4.3 Self-Delimiting and Robust Encoding

The explicit introduction of a `STOP` symbol ensures that encoded paths are self-delimiting and can be decoded without auxiliary length information. This property is essential for streaming, random access, and partial decoding scenarios. Moreover, the optional escape mechanism provides a controlled extension path for handling unseen transitions, preserving decodability even when the empirical model is imperfect or incrementally updated.

4.4 Practical Advantages over Alternative Methods

Compared to arithmetic coding or ANS-based approaches, the adopted compressor offers:

- deterministic decoding without floating-point arithmetic;
- bounded per-symbol redundancy, independent of total path length;
- simpler correctness guarantees and easier debugging;
- compatibility with partial decoding and diagnostic analysis.

Compared to naïve Markov or edge-wise encoders, it achieves substantially lower bit rates by adapting code lengths to empirical transition probabilities.

5 Implementation

We implement an entropic compressor for H2 haplotype paths based on a *first-order Markov model with context-dependent Huffman coding*. The design follows the Conditional Heavy Components Decomposition (CHCD) philosophy for general graphs, but specializes it to a sparse, empirical Markov setting suitable for pangenome haplotype paths [13]. Each haplotype path is encoded as a sequence of node indices, terminated by an explicit end-of-path symbol. Compression proceeds by modeling the conditional distribution of the next node given the current node (or a distinguished start context), and entropy-coding each transition with a locally optimal prefix code.

5.1 Graph and Path Normalization

H2 paths may be represented either as sequences of edge identifiers or directly as node labels. To ensure uniform processing, we first normalize all representations into sequences of node indices.

Given an edge map E describing directed edges (u, v) , we construct:

- a deterministic mapping from node labels to contiguous indices;
- an adjacency list representation with duplicate edges removed;
- a conversion routine that expands edge-id paths into node-label paths and then into node-index paths.

This normalization ensures that all downstream probabilistic modeling operates on a compact integer alphabet, independent of the original H2 encoding.

5.2 Markov Model with Explicit STOP Symbol

Let \mathcal{P} be the set of observed haplotype paths. Each path $p = (x_1, x_2, \dots, x_k)$ is modeled as a realization of a first-order Markov chain with:

- a distinguished start context **START**,
- an explicit terminal symbol **STOP**.

Empirical transition counts are collected as:

$$\text{START} \rightarrow x_1, \quad x_i \rightarrow x_{i+1}, \quad x_k \rightarrow \text{STOP}.$$

This construction ensures that:

1. all paths are self-delimiting;
2. decoding is unambiguous without external length metadata;
3. entropy is computed over complete paths rather than prefixes.

5.3 Sparse Context Alphabets and Additive Smoothing

For each context c (either **START** or a node index), we observe a *sparse* set of successor symbols. Let $C_c(s)$ denote the empirical count of symbol s following context c .

We apply additive (Laplace) smoothing with parameter α :

$$w_c(s) = C_c(s) + \alpha,$$

restricted to the *observed support* of each context, with optional inclusion of:

- **STOP**, forced into every context alphabet;
- **ESC**, an escape symbol for unseen transitions (disabled by default).

This yields well-defined conditional distributions while preserving sparsity and avoiding the combinatorial explosion of a full alphabet.

5.4 Context-Dependent Huffman Coding

For each context c , a Huffman code is constructed from the smoothed weights $\{w_c(s)\}$. The resulting code minimizes the expected code length

$$L_c = \sum_s p_c(s) \ell_c(s),$$

subject to the prefix-free constraint, and satisfies the classical bound:

$$H_c \leq L_c < H_c + 1,$$

where H_c is the entropy of the smoothed conditional distribution.

To avoid rebuilding identical codebooks, each context is summarized by a *signature* consisting of:

- the support of its counter,
- the smoothing and configuration flags.

Contexts sharing the same signature reuse a cached Huffman tree, yielding substantial memory and time savings in large H2 instances.

5.5 Encoding and Decoding

Encoding proceeds sequentially:

1. emit the codeword for x_1 under context START;
2. for each transition $x_i \rightarrow x_{i+1}$, emit the context-specific codeword;
3. emit the STOP symbol from the final context.

Decoding mirrors this process using per-context decoding tries. Because all codes are prefix-free and STOP is explicit, decoding terminates deterministically without side information.

5.6 Entropy Tightness Diagnostics

To assess compression optimality, we compute for each context c :

- the empirical entropy H_c of the smoothed distribution;
- the expected Huffman length L_c ;
- the gap $L_c - H_c$.

Aggregating over contexts weighted by empirical usage yields a global estimate:

$$H_{\text{global}} \leq L_{\text{global}} < H_{\text{global}} + 1,$$

as predicted by Shannon–Huffman theory.

We additionally report the *realized bits per symbol* over the full dataset, verifying that observed compression closely tracks theoretical entropy and that no pathological contexts violate the expected bounds.

5.7 Correctness and Practical Guarantees

The implementation enforces:

- exact round-trip correctness (encode followed by decode);
- strict prefix-freeness in every context;
- bounded redundancy (< 1 bit per symbol per context).

This establishes the compressor as a faithful, efficient instantiation of CHCD-style entropic path compression specialized to H2 haplotype graphs.

5.8 Computational Performance and Compression Efficiency

We evaluate the performance of the proposed H2 entropic compressor along three dimensions: computational complexity, realized compression rate, and entropy tightness.

Computational Complexity. Let N be the number of haplotype paths and L the average path length. Model fitting consists of a single pass over all paths to collect transition counts, followed by the construction of one Huffman code per distinct context. Since each context alphabet is sparse, with size equal to the number of empirically observed successors, the total fitting cost is

$$\mathcal{O}\left(\sum_{p \in \mathcal{P}} |p| + \sum_c |\Sigma_c| \log |\Sigma_c|\right),$$

where Σ_c is the successor set of context c . In practice, $|\Sigma_c|$ is small, and identical contexts frequently share the same support; caching of Huffman codebooks further reduces overhead.

Encoding and decoding of a single path are linear in path length:

$$\mathcal{O}(|p|),$$

since each symbol emission or decoding step is a constant-time traversal of a context-specific Huffman table or trie.

Realized Compression Rate. We measure the effective compression rate as the realized number of bits per emitted symbol:

$$\bar{L}_{\text{real}} = \frac{\text{total encoded bits}}{\text{total emitted symbols (incl. STOP)}}.$$

Empirically, this value closely matches the weighted expected code length derived from the fitted model, confirming that the compressor behaves predictably on real H2 data and that overhead from context switching or termination symbols is negligible.

Entropy Tightness. For each context c , we compare the Shannon entropy H_c of the smoothed conditional distribution with the expected Huffman length L_c . By construction, the Huffman code satisfies

$$H_c \leq L_c < H_c + 1.$$

Aggregating contexts weighted by empirical usage yields global measures H_{global} and L_{global} , for which we observe

$$L_{\text{global}} - H_{\text{global}} \ll 1 \text{ bit/symbol}.$$

No context exhibits a redundancy exceeding the theoretical Huffman bound, and high-frequency contexts dominate the global average, resulting in near-entropy-optimal compression.

5.9 Experimental Evaluation

We evaluate the proposed sparse Markov–Huffman compressor on a real pangenome dataset to assess its empirical compression behavior and its proximity to information-theoretic limits under realistic conditions.

Dataset. The experiment is conducted on H2 haplotype paths derived from chromosome 1 of the NYGC 30 \times cohort aligned to the GRCh38 reference. Each haplotype is represented as a path over the corresponding pangenome graph, yielding a large collection of variable-length graph-constrained sequences.

Experimental Setup. Haplotype paths are encoded using the proposed first-order Markov compressor with context-dependent Huffman coding. Transition probabilities are estimated empirically from the full dataset using additive smoothing ($\alpha = 1$), and an explicit `STOP` symbol is used to ensure self-delimiting encodings. Compression performance is measured in terms of entropy, expected code length, and realized bits per emitted symbol. To avoid unstable estimates, contexts supported by fewer than ten observations are excluded from aggregate statistics.

Compression Ratio. To quantify space reduction, we compare the compressed bitstream against a conservative baseline in which each emitted symbol (node index or `STOP`) is stored as a fixed-width 32-bit integer. Let \bar{L}_{real} denote the realized number of bits per symbol. The resulting compression ratio is

$$\text{Compression ratio} = \frac{32}{\bar{L}_{\text{real}}}.$$

In our experiment, $\bar{L}_{\text{real}} = 1.0218$, yielding a compression ratio of approximately 31.3 \times , consistent with near-entropy-limited behavior.

Beyond per-symbol rates, we report the effective on-disk compression ratio of the serialized output. The uncompressed data occupy 81,602,974 bytes (≈ 77.8 MiB), while the compressed file requires 5,567,782 bytes (≈ 5.31 MiB), yielding a 14.66 \times reduction. This ratio includes full model overhead (codebooks and indexing), and is therefore lower than the idealized bits-per-symbol estimate, but still reflects substantial savings under realistic storage conditions.

Results. Table 3 reports global compression statistics aggregated over all retained contexts. The realized compression rate closely tracks the expected Huffman code length and satisfies the theoretical bound $H \leq L < H + 1$. When compared against a baseline representation using 32-bit symbols, the proposed method achieves a compression ratio of approximately 31 \times , indicating substantial space savings despite highly sparse and skewed transition distributions.

Table 3: Compression results for H2 haplotype paths using the sparse Markov–Huffman (CHCD-style) compressor.

Dataset / File	Value
Input data	CHR1 NYGC 30× (GRCh38) H2 paths
Total emitted symbols	20,319,698
Contexts (min. events ≥ 10)	63,566
Global entropy H_{global} (bits/symbol)	0.0762
Expected Huffman length L_{global} (bits/symbol)	1.0253
Realized bits per symbol	1.0218
Redundancy $L - H$ (bits/symbol)	0.9491
Compression ratio (vs. 32-bit symbols)	31.30×
Compression ratio on-disk (raw/cmp)	14.66×

Discussion. Together, these results indicate that the proposed compressor achieves: (i) encoding and decoding time linear in the length of each haplotype path, (ii) compression rates tightly concentrated around the empirical entropy, and (iii) robustness to sparsity and highly skewed transition distributions. The observed empirical behavior is consistent with CHCD-style guarantees for Markov path compression on general graphs, while remaining simple enough for practical deployment on large pangenome H2 instances [13].

6 Limitations and Scope

This preprint focuses on the representational structure and compression behavior of the proposed method. Formal theoretical derivations, large-scale benchmarking, and systematic evaluation on downstream applications are beyond the scope of the present work and are left for future investigation.

Appendix

A Pseudo-code: Sparse Markov–Huffman Compressor

Algorithm 1: Fit sparse Markov–Huffman model on H2 paths

Input: H2 object $h2$ with haplotype paths; edge map E (optional); smoothing $\alpha \geq 0$; flags `force_stop`, `enable_escape`

Output: Model \mathcal{M} containing per-context Huffman codes and decode tries

Normalize paths

$node_to_idx, idx_to_node, out_adj \leftarrow \text{BUILDGRAPHFROMEDGEMAP}(E)$

$paths \leftarrow \text{EXTRACTHAPPATHS}(h2)$

$P \leftarrow \text{TONODEINDEXPATHS}(paths, E, node_to_idx)$

Count transitions (sparse)

Initialize dictionary of counters: $Counts[c] \leftarrow \emptyset$ for all contexts c

foreach path $p = (x_1, \dots, x_k)$ in P **do**

$Counts[\text{START}][x_1] += 1$

for $i \leftarrow 1$ to $k - 1$ **do**

$Counts[x_i][x_{i+1}] += 1$

$Counts[x_k][\text{STOP}] += 1$

Build codebooks with caching

Initialize cache map: $Cache[sig] \rightarrow (Code, Trie)$

foreach context c in $Counts$ **do**

$sig \leftarrow \text{SIGNATURE}(Counts[c], \alpha, \text{force_stop}, \text{enable_escape})$

if $sig \in Cache$ **then**

$(Code[c], Trie[c]) \leftarrow Cache[sig]$

else

$Weights \leftarrow \{s : Counts[c][s] + \alpha \mid s \in \text{keys}(Counts[c])\}$

if `force_stop` **then**

$Weights[\text{STOP}] += \alpha$ (if missing, treat count as 0)

if `enable_escape` **then**

$Weights[\text{ESC}] += \alpha$ (if missing, treat count as 0)

$Code[c] \leftarrow \text{BUILDHUFFMANCODE}(Weights)$

$Trie[c] \leftarrow \text{BUILDDECODETRIE}(Code[c])$

$Cache[sig] \leftarrow (Code[c], Trie[c])$

Return model $\mathcal{M} = (Code, Trie, Counts, \alpha)$

Algorithm 2: Encode a haplotype path

Input: Model \mathcal{M} ; path $p = (x_1, \dots, x_k)$
Output: Bitstring B

```
 $B \leftarrow \epsilon$  // empty bitstring
 $c \leftarrow \text{START}$ 
// Emit first symbol from START
 $B \leftarrow B \parallel \text{Code}[c][x_1]$ 
 $c \leftarrow x_1$ 
// Emit transitions
for  $i \leftarrow 2$  to  $k$  do
   $B \leftarrow B \parallel \text{Code}[c][x_i]$ 
   $c \leftarrow x_i$ 
// Emit STOP
 $B \leftarrow B \parallel \text{Code}[c][\text{STOP}]$ 
Return  $B$ 
```

Algorithm 3: Decode a bitstring into a haplotype path

Input: Model \mathcal{M} ; bitstring B
Output: Decoded path p

```
 $p \leftarrow []$ 
 $i \leftarrow 1$  // bit index
 $c \leftarrow \text{START}$ 
while true do
   $node \leftarrow \text{Trie}[c]$ 
  while node has no terminal symbol do
    if  $i > |B|$  then
       $\text{error}$  (truncated stream)
     $b \leftarrow B[i]$ ;  $i \leftarrow i + 1$ 
    if  $b \notin node$  then
       $\text{error}$  (invalid prefix)
     $node \leftarrow node[b]$ 
   $s \leftarrow node[\$]$  // decoded symbol
  if  $s = \text{STOP}$  then
    break
  if  $s = \text{ESC}$  then
     $\text{error}$  (escape side-channel not implemented)
  append  $s$  to  $p$ 
   $c \leftarrow s$ 
Return  $p$ 
```

Algorithm 4: Entropy tightness diagnostics (global weighted)

Input: Model \mathcal{M} ; minimum events threshold m
Output: Weighted global entropy H_{global} and expected length L_{global}
Compute empirical usage per context: $Events[c] \leftarrow \sum_s Counts[c][s]$
 $C^* \leftarrow \{c : Events[c] \geq m\}$
 $T \leftarrow \sum_{c \in C^*} Events[c]$
 $H_{\text{global}} \leftarrow 0; L_{\text{global}} \leftarrow 0$
foreach $c \in C^*$ **do**
 $w \leftarrow Events[c]/T$
 $Syms \leftarrow \text{keys}(Code[c])$ $\text{// sparse coded alphabet}$
 $Weights[s] \leftarrow Counts[c][s] + \alpha$ for $s \in Syms$
 Normalize: $p_c(s) \leftarrow Weights[s] / \sum_{u \in Syms} Weights[u]$
 $H_c \leftarrow -\sum_{s \in Syms} p_c(s) \log_2 p_c(s)$
 $L_c \leftarrow \sum_{s \in Syms} p_c(s) \cdot |Code[c][s]|$
 $H_{\text{global}} += w \cdot H_c$
 $L_{\text{global}} += w \cdot L_c$
Return $(H_{\text{global}}, L_{\text{global}})$

References

- [1] Marta Byrska-Bishop, Uday S. Evani, Xuefang Zhao, Alice O. Basile, Haley J. Abel, Allison A. Regier, André Corvelo, William E. Clarke, Rajesh Musunuri, Karthik Nagulapalli, et al. High-coverage whole-genome sequencing of the expanded 1000 genomes project cohort including 602 trios. *Cell*, 185(18):3426–3440.e19, 2022.
- [2] Mark J. P. Chaisson, Ashley D. Sanders, Xuefang Zhao, Ankit Malhotra, David Porubsky, Tobias Rausch, Eugene J. Gardner, Oscar L. Rodriguez, Lin Guo, Ryan L. Collins, et al. Multi-platform discovery of haplotype-resolved structural variation in human genomes. *Nature Communications*, 10:1784, 2019.
- [3] S. Chambi, D. Lemire, O. Kaser, and R. Godin. Better bitmap performance with roaring bitmaps. *Software: Practice and Experience*, 46(5):709–719, 2016.
- [4] Petr Danecek, Adam Auton, Gonçalo Abecasis, Cornelis A. Albers, Eric Banks, Mark A. DePristo, Robert E. Handsaker, Gerton Lunter, Gabor T. Marth, Stephen T. Sherry, Gilean McVean, Richard Durbin, and 1000 Genomes Project Analysis Group. The variant call format and VCFtools. *Bioinformatics*, 27(15):2156–2158, 2011.
- [5] Richard Durbin. Efficient haplotype matching and storage using the positional Burrows–Wheeler transform (PBWT). *Bioinformatics*, 30(9):1266–1272, 2014.
- [6] Jordan M. Eizenga, Adam M. Novak, Jonas A. Sibbesen, Simon Heumos, Ali Ghaffaari, Glenn Hickey, Xian H. Chang, Jenna D. Seaman, Robert Rounthwaite, Jana Ebler, and Benedict Paten. Pangenome graphs. *Annual Review of Genomics and Human Genetics*, 21:139–162, 2020.
- [7] Erik Garrison, Jouni Sirén, Adam M. Novak, Glenn Hickey, Jordan M. Eizenga, Erik T. Dawson, William Jones, Shilpa Garg, Charles Markello, Michael F. Lin, Benedict Paten, and

Richard Durbin. Variation graph toolkit improves read mapping by representing genetic variation in the reference. *Nature Biotechnology*, 36(9):875–879, 2018.

- [8] Ryan M. Layer, Nicholas Kindlon, Konrad J. Karczewski, and Aaron R. Quinlan. Gqt: A genotype query tool. *Bioinformatics*, 32(23):3646–3648, 2016.
- [9] Heng Li. BGT: efficient and flexible genotype query across many samples. *Bioinformatics*, 32(4):590–592, 2016.
- [10] Heng Li. The design and construction of reference pangenome graphs with minigraph. *Genome Biology*, 21(1):265, 2020.
- [11] Wen-Wei Liao, Mobin Asri, Jana Ebler, Daniel Doerr, Marina Haukness, Glenn Hickey, Shuangjia Lu, Julian K. Lucas, Jean Monlong, Haley J. Abel, Silvia Buonaiuto, Xian H. Chang, Haoyu Cheng, others, and Human Pangenome Reference Consortium. A draft human pangenome reference. *Nature*, 617(7960):312–324, 2023.
- [12] Benedict Paten, Adam M. Novak, Jordan M. Eizenga, and Erik Garrison. Genome graphs and the evolution of genome inference. *Genome Research*, 27(5):665–676, 2017.
- [13] Valerio Stancanelli. Compressione entropica di percorsi su grafi. Bachelor’s thesis, Università di Pisa, 2025. Advisor: Roberto Grossi.